Robust Hyperspectral Unmixing in the Presence of Mixed Noise using Joint Sparsity and Total Variation Regularization

Kukkala Prasanna Kumari[1], K Anuradha[2], Grandhi Adhilakshmi[3]

[1,2,3]Assistant Professor, Department of ECE, Malla Reddy Engineering College and Management Sciences, Hyderabad, Telangana.

Abstract

Hyperspectral unmixing is a vital process in hyperspectral imaging, aiming to estimate constituent endmembers and their fractional abundances within each pixel. Hyperspectral images are often marred by various noise sources. This research delves into the hyperspectral unmixing challenge in a general scenario that accounts for mixed noise, explicitly addressing Gaussian noise and sparse noise. The unmixing model is tailored to harness the joint sparsity of abundance maps, enabling the robust separation of endmembers and abundances from noise. Additionally, a total-variation-based regularization technique is incorporated to capture the smoothness of abundance maps, further enhancing the accuracy of the unmixing process in noisy hyperspectral images.

Keywords: Hyperspectral Unmixing, Noise, Gaussian Noise, Sparse Noise, Joint Sparsity, Total Variation Regularization.

1. Introduction

Hyperspectral unmixing in remote sensing is a traditional, essential, and challenging topic. It is a challenge to classify endmembers and their fractions in a hyperspectral image at each pixel [1]. The word terminus refers to different materials that may be found in a hyperspectral frame directly or indirectly. The term direct refers to clear pixels being included and mixed pixels being indirectly included. In a satellite image, a pixel is the same as a large space area on earth. This area of space constitutes a single entity or numerous objects occupied by the pixel [2]. If the pixel surface forms a single object, then the mixed pixel is referred to as a pure pixel or mixed pixel. The term fractional excess refers to the proportion of the end element that is present in a pixel. Therefore, an abundance map indicates how a single endpiece is spread throughout an area [3]. There is a fractional abundance of pure pixels, while the fractional abundance of mixed pixels is between zero and one pixel. Hyperspectral unmixing is used in several fields, such as geology, agriculture, environmental sciences, biology and so on. Abundance maps are widely used as vectors for other hyperspectral image implementations in image analysis and pattern recognition [4]. Hyperspectral unmixing is also used in applications for de-noising, data fusion, and super-resolution. There are, however, some nonlinear models for hyperspectral unmixing based on the unmixing method of linear mixing. This statement could not always be valid, and thus it is not this assumption that depends on this work [5]. The use of existing spectral libraries as well as of others which aim to calculate endmember spectral signatures using techniques based on factorization of non-negative matrixes can be classified as the one using existing spectral libraries for several endmember categories including artificial, mineral, soil, etc [6]. This work is based on Vertical line stripes are typically seen on images collected by sensors of the push-broom type that record scene in the direction of flight. Some defective pixels are creating a shot noise.

The unmixing of hyperspectral images is ideal, even if one or more of these sources of noise distort them [7]. A denoisers algorithm followed by unmixing algorithms will first be used to solve this problem of unmixing with mixed tone. This analysis varies both in the noise model and in the solution approach from those current methods [8]. This work uses the noise model that was later used to

denoise. This model enables one to formulate a linear hyperspectral unmixing problem which specifically takes Gaussian as well as sparse noise into account. It comprises stripes, noise from the shot as well as noise from impulse. There are tremendous members from various spectral libraries (e.g., USGS), but only a few of them are contained in the hyperspectral image [9]. The number of end members accessible is large. A subset of the end members is present at each pixel (present in the entire picture). The strong spatial similarity of natural pictures also means that there may be pixels with the same spectral signature in this area. This finding can be modelled on abundance maps as a total variance regularisation [10]. Our analysis enhances SR and its versions of total uncertainty spatial regularisation (SRTV) and collaborative SR (CLSR), focused on state-of- the art scarce regression (SR).

Rest of the paper is organized as follows: Section 2 details about literature survey, section 3 details about the proposed methodology, section 4 details about the results with discussion, and section 5 concludes article with references.

2. Literature Survey

Iordache, et al. (2010) [11] explored the applicability of new sparse algorithms to perform spectral unmixing of hyperspectral images using available spectral libraries instead of resorting to well-known end member extraction techniques widely available in the literature. Our main assumption is that it is unlikely to find pure pixels in real hyperspectral images due to available spatial resolution and mixing phenomena happening at different scales. Quintano, Carmen et al. (2012) [12] proposed satellite imagery which is formed by finite digital numbers representing a specific location of ground surface in which each matrix element is denominated as a picture element or pixel. The pixels represent the sensor measurements of spectral radiance. The radiance recorded in the satellite images is then an integrated sum of the radiances of all targets within the instantaneous field of view (IFOV) of the sensors. Jamshid Moghadam et al. (2020) [13] aims to give an overview of most nonlinear mixing models and methods used in hyperspectral image processing, and many recent developments in this field. Besides, several of the more popular nonlinear unmixing techniques are explained in detail. In this regard, nonlinear unmixing methods can be categorized into two groups: physics-based methods and data-driven techniques. The most important methods of these two groups are divided into bilinear and multi-linear models, intimate mineral mixture models, radiosity based approaches, ray tracing, neural network, kernel methods, manifold learning, and topology methods. Wang, Le et al. (2016) [14] proposed the incorporation of spatial information has drawn increasing attention in multispectral and hyperspectral data analysis. In particular, the property of spatial autocorrelation among pixels has shown great potential for improving understanding of remotely sensed imagery. He provided a comprehensive review of the state-of-the-art techniques in incorporating spatial information in image classification and spectral unmixing. Hong, Danfeng et al. (2018) [15] proposed the hyperspectral imagery collected from airborne or satellite sources inevitably suffers from spectral variability, making it difficult for spectral unmixing to accurately estimate abundance maps. The classical unmixing model, the linear mixing model (LMM), generally fails to handle this sticky issue effectively. To this end, they proposed a novel spectral mixture model, called the augmented LMM, to address spectral variability by applying a data-driven learning strategy in inverse problems of hyperspectral unmixing.

Wan, Lulu, et al. (2021) [16] they presented a comprehensive survey of the NMF-based methods proposed for hyperspectral unmixing. Taking the NMF model as a baseline, they show how to improve NMF by utilizing the main properties of HSIs (e.g., spectral, spatial, and structural information). they categorize three important development directions, including constrained NMF, structured NMF, and generalized NMF. Halimi, Abderrahim, et al. (2016) [17] presented three

hyperspectral mixture models jointly with Bayesian algorithms for supervised hyperspectral unmixing. Based on the residual component analysis model, the proposed general formulation assumes the linear model to be corrupted by an additive term whose expression can be adapted to account for nonlinearities (NLs), endmember variability (EV), or mismodeling effects (MEs). He, Wei, et al. (2017) [18] have proposed the Blind hyperspectral unmixing (HU), which includes the estimation of endmembers and their corresponding fractional abundances, is an important task for hyperspectral analysis. Recently, nonnegative matrix factorization (NMF) and its extensions have been widely used in HU. Unfortunately, most of the NMF-based methods can easily lead to an unsuitable solution, due to the nonconvexity of the NMF model and the influence of noise. Zhao, Min et al. (2021) [19] have proposed the spectral unmixing which a widely used technique in hyperspectral image was processing and analysis. It aims to separate mixed pixels into the component materials and their corresponding abundances. Early solutions to spectral unmixing are performed independently on each pixel. Nowadays, investigating proper priors into the unmixing problem has been popular as it can significantly enhance the unmixing performance. Zhou, Lei, et al (2020) [20] Hyperspectral unmixing is a crucial task for hyperspectral images (HSIs) processing, which estimates the proportions of constituent materials of a mixed pixel. Usually, the mixed pixels can be approximated using a linear mixing model. Since each material only occurs in a few pixels in real HSI, sparse nonnegative matrix factorization (NMF), and its extensions are widely used as solutions.

3. Proposed Methodology

3.1 Problem description and formulation

This section describes how linear unmixing problem can be mathematically formulated as sparse recovery problem followed by our proposed problem formulation.

3.1.1 Notations

Let I_n represents identity matrix of size $n \times n$. The operation $x = vec(X)$ represents vectorization operation on matrix X with columns appended whereas $X = mat(x)$ represents its inverse operation. A hyperspectral data cube of size $m \times n \times b$ can be represented as a matrix of size $b \times p$ where b is the total number of bands and $p = m \times n$ is the total number of pixels in the image. $M \in \mathbb{R}^{b \times e}$ represents mixing matrix also called endmember matrix in which each column represents spectral signature of an endmember. Let $\nabla = \begin{pmatrix} \nabla_h \\ \nabla_v \end{pmatrix}$ be total variation operator with ∇_h and ∇_v representing horizontal and vertical total-variation operators, respectively, with $(\nabla_h X)_{i,j} = X_{i,j+1} - X_{i,j}$ and $(\nabla_v X)_{i,j} = X_{i+1,j} - X_{i,j}$. The $l_{2,1}$-norm of a matrix $A \in \mathbb{R}^{M \times N}$ is defined as

$$\|A\|_{2,1} = \sum_{i=1}^{M} \|\overrightarrow{a_i}\|_2 = \sum_{i=1}^{M} \sqrt{\sum_{j=1}^{N} a_{ij}^2} \tag{1}$$

Whereas Frobenius norm and l_1 −norm of a matrix is defined as follows:

$$\|A\|_F^2 = \sum_{i=1}^{M} \sum_{j=1}^{N} a_{ij}^2, \quad \|A\|_1 = \sum_{i=1}^{M} \sum_{j=1}^{N} |a_{i,j}| \tag{2}$$

3.1.2 Problem Description

The linear unmixing problem for a pixel in the presence of Gaussian noise is represented as constrained linear regression model.

$$y = Ma + n, \quad \|a\|_1 = 1, \quad a_i \geq 0 \; \forall i \tag{3}$$

where $y \in R^b \times 1$ is a pixel vector in b spectral bands, M is a mixing matrix with e number of endmembers as column vectors, $a \in R^e \times 1$ is called abundance vector that represents the fraction of each endmember used in the formation of that pixel, and n represents Gaussian noise which accounts for various external environmental factors. The constraint $\|a\|_1 = 1$ represents abundance sum-to-one constraint to ensures that total contribution of each endmember in formation of a pixel is one. As it has been noticed in [7], [21], and [22], all the endmembers present in a real hyperspectral image may not be available in the spectral library. Therefore, abundance sum may not be exactly equal to one. Also, if this constraint of $\|a\|_1 = 1$ is enforced then formulating the l_1-norm minimization problem on a will be meaningless. Therefore, this work does not enforce this constraint in the problem formulation. The abundance nonnegativity constraint represents that contribution cannot be negative.

Since mixing matrix is known for hundreds of most used materials. Therefore, generally $e > b$ and eq. (3) is an underdetermined system of linear equations. In general, an underdetermined system has infinite solutions; therefore, we need additional constraints on the variable a to determine it uniquely. The observation that a pixel is mixture of very few endmembers as opposed to hundreds of available endmembers allow us to treat abundance vector a as sparse vector thus unmixing can be recast as compressed sensing [23], [24] problem.

$$\min_a \|y - Ma\|_2^2 \text{ subject to } \|a\|_0 \leq k \tag{4}$$

where k is the sparsity of a, i.e., maximum number of nonzero elements of a. This is an NP-hard [25] problem whose solution can be approximated using greedy pursuit algorithms such as OMP [26], StOMP [27], CoSAMP [28], etc. It has been shown that under certain conditions solution of the NP-hard problem eq. (4) can be approximated by solving its convex surrogate l_1-norm minimization problem.

$$\min_a \|y - Ma\|_2^2 + \lambda \|a\|_1 \tag{3}$$

This problem is a convex optimization problem, and various algorithms have been proposed in literature SPGL1 [29], FISTA [30], NESTA [31], Bregman Iteration [32], etc., to solve this problem. The unmixing model in eq. (3) can be extended for all the pixels as

$$Y = MA + N, \quad A \geq 0 \tag{4}$$

where $Y \in \mathbb{R}^{b \times p}$ is a matrix with p pixels as column vectors, $A \in \mathbb{R}^{e \times p}$ is sparse abundance matrix, and N is Gaussian noise. This unmixing model can be though of as specialization of image denoising model.

$$Y = X + N \tag{5}$$

where $X \in \mathbb{R}^{b \times p}$ and $X = MA$ is clean hyperspectral image which imply that unmixing can lead to denoising provided that mixing matrix is known.

3.1.3 Proposed Formulation

A real hyperspectral image may contain a mixture of Gaussian and sparse noise; therefore, we consider the mixed noise model for unmixing and account for both types of noise. The usual unmixing model in eq. (4) can be extended as

$$Y = MA + S + G, \quad A \geq 0 \tag{6}$$

here S and G represents sparse and Gaussian noise, respectively. The above noise model assumes both Gaussian and sparsenoise to be additive noise. Sparse noise accounts for horizontal or vertical line strips, shot noise and any impulse noise present in a hyperspectral image. All these kinds of noise are termed as sparse noise since they corrupt few pixels in a hyperspectral image. By utilizing this model, we can formulate the unmixing problem as

$$\min_{A,S} \|Y - MA - S\|_F^2 + \lambda_1 \|A\|_{2,1} + \lambda_2 \|S\|_1 \tag{7}$$

Here, the first term is data fidelity term that is equivalent to minimizing the variance of Gaussian noise $G = Y - MA - S$. First regularization term is an $l_{2,1}$-norm minimization term on abundance matrix A which is also called joint-sparse regularization term. This term is based on the observation that in most hyperspectral images, fewer endmembers are present compared to the available endmembers. This observation is mathematically modeled as joint-sparse regularization on matrix A with few nonzero rows, but each nonzero row can be dense. The second regularization term corresponds to minimizing l_1-norm of sparse noise matrix S. Here, l_1-norm is minimized due to modelling assumption that sparse noise affects few pixels in the image. As an alternative unmixing model, we can also exploit the fact that most natural images are piece-wise smooth, e.g., if there are some vegetation pixels in the image the nearby pixels are also likely to be vegetation pixels. Therefore, the abundance maps can be considered as piecewise smooth. The piecewise smoothness can be modeled as total-variation regularization [16].

$$\min_{A,S} ||Y - MA - S||_F^2 + \lambda_1 ||\nabla A^T||_1 + \lambda_2 \|S\|_1 \tag{8}$$

Here, ∇ is two-dimensional (2-D) total-variation operator that applies total variation along both horizontal and vertical directions on a 2-D image. The operator ∇ is applied on A^T because each abundance map is along rows of A. In this work, we propose to simultaneously exploit both the joint sparsity as well as spatial smoothness of the abundance maps in the light of generic noise model. Thus, the proposed hyperspectral unmixing problem formulation can be expressed as

$$\min_{A,S} ||Y - MA - S||_F^2 + \lambda_1 ||\nabla A^T||_1 + \lambda_2 \|A\|_{2,1} + \lambda_3 \|S\|_1 \tag{9}$$

Here, λ_1, λ_2, and λ_3 are regularization parameters corresponding to total-variation term, joint-sparsity term, and sparse noise term, respectively. These three models in eq. (7)-(9) estimate $X = MA$ be the clean image then we can get denoised image $\hat{X} = M\hat{A}$ where $\hat{A}$ is the estimated abundance maps by solving eq. (9). Along with generic noise model eq. (6), we have exploited both joint sparsity as well as piecewise smoothness of abundance maps. We are not aware of any efficient algorithm to solve eq. (9); therefore, in the next section, we briefly describe how to solve this problem using the split-Bregman [17] based technique.

3.2 Proposed Algorithm

This section describes how the split-Bregman [17] approach can be utilized to derive the algorithm for solving eq. (9). The split Bregman approach is suitable to solve eq. (8) because it has been designed to handle multiple regularization terms. The variable A is not separable in eq. (9); therefore, we utilize auxiliary variables P and Q to make the problem separable. Set $P = \nabla A^T$ and $Q = A$, then we get following constrained problem:

$$\begin{aligned} \underset{A,S,P,Q}{\text{minimize}} \quad & \|Y - MA - S\|_F^2 + \lambda_1\|P\|_1 + \lambda_2\|Q\|_{2,1} + \lambda_3\|S\|_1 \\ \text{subject to} \quad & P = \nabla A^T \\ & Q = A. \end{aligned} \tag{10}$$

This problem can be rewritten into unconstrained form by using two Bregman variables B_1 and B_2 to get

$$\begin{aligned} \underset{A,S,P,Q}{\text{minimize}} & \|Y - MA - S\|_F^2 + \lambda_1\|P\|_1 + \lambda_2\|Q\|_{2,1} + \lambda_3\|S\|_1 \\ & + \mu_1\|P - \nabla A^T - B_1\|_F^2 + \mu_2\|Q - A - B_2\|_F^2 \end{aligned} \tag{11}$$

Where B_1 and B_2 are updated as

$$\begin{aligned} B_1 &= B_1 + \nabla A^T - P \\ B_2 &= B_2 + A - Q. \end{aligned} \tag{12}$$

Above problem is separable in each variable therefore can be written into following subproblems as

$$\begin{aligned} \text{P1:} \quad & \min_P \ \mu_1\|P - \nabla A^T - B_1\|_F^2 + \lambda_1\|P\|_1 \\ \text{P2:} \quad & \min_Q \ \mu_2\|Q - A - B_2\|_F^2 + \lambda_2\|Q\|_{2,1} \\ \text{P3:} \quad & \min_S \ \|Y - MA - S\|_F^2 + \lambda_3\|S\|_1 \\ \text{P4:} \quad & \min_A \ \|Y - MA - S\|_F^2 + \mu_1\|P - \nabla A^T - B_1\|_F^2 \\ & + \mu_1\|Q - A - B_2\|_F^2 \end{aligned} \tag{14}$$

each of these problems can be solved iteratively by using Bregman iteration with Bregman variables updated in kth iteration as

$$\begin{aligned} B_1^{k+1} &= B_1^k + \nabla(A^k)^T - P^k \\ B_2^{k+1} &= B_2^k + A^k - Q^k. \end{aligned} \tag{15}$$

The problems P1 and P3 are of the form.

$$\|y - x\|_2^2 + \lambda\|x\|_1 \tag{16}$$

which can be solved by using soft thresholding [33] operation

$$\hat{x} = \mathbf{SoftTh}(y, \lambda) = \mathbf{sign}(y) \times \max\left\{0, |y| - \frac{\lambda}{2}\right\} \tag{17}$$

The problem P2 can be solved by using the procedure as described in [15, Sec. 3.3.3]. This is a l_2-norm shrinkage operation on each row $q^{(i)}\ \forall i = 1,2,\ldots,e$, of matrix Q. The l_2-norm shrinkage problem is

$$\min_x \|y - x\|_2^2 + \lambda\|y\|_2 \tag{18}$$

whose solution is given by

$$\hat{x} = \text{Shrink}(y, \lambda) = \max\left\{\|y\|_2 - \frac{\lambda}{2}, 0\right\} \odot \frac{y}{\|y\|_2} \tag{19}$$

here $\odot$ represent element by element multiplication operation with the assumption that $0 \times \frac{0}{0} = 0$. The problem P4 is a differentiable convex optimization problem. After differentiating we get following linear system of equations with variable A:

$$\begin{aligned} &M^T M A + \mu_1 A \nabla^T \nabla + \mu_2 A \\ &\quad = M^T (Y - S) + \mu_1 (P^T - B_1^T)\nabla + \mu_2 (Q - B_2) \end{aligned} \tag{20}$$

This equation can be rewritten as

$$\begin{aligned} &\Psi a = vec(M^T (Y - S)) + \alpha \quad \text{where} \\ &\Psi = (I_c \otimes M^T M)\mu_1 (\nabla^T \nabla \otimes I_c) + \mu_1 I_{pc} \\ &\alpha = \mu_1 (P^T - B_1^T)\nabla + \mu_2 (Q - B_2)). \end{aligned} \tag{21}$$

The above system of linear equations is large and sparse whose solution can be approximated using algorithms such as LSQR [34]. Algorithm 1 outlines the steps of proposed jointly sparse and total-variation regularized hyperspectral unmixing algorithm using the split-Bregman approach. We use the acronym JSTV for the proposed joint sparsity and total variation-based unmixing method. By setting λ_1=0, we can derive the solution of eq. (15) which we refer as split-Bregman algorithm-based joint-sparse regularized (SBJS) unmixing algorithm. Similarly, λ_2=0 results in an algorithm that solves eq. (16) which we refer as split-Bregman algorithm based total variation regularized (SBTV) unmixing algorithm.

Algorithm 1. Proposed JSTV Algorithm for solving (8)

input: $Y, \lambda_1, \lambda_2, \mu_1, \mu_2$, innerIter, outerIter
output: $\hat{A}$ (Abundance maps).
For $j = 1$ to outerIter **do**
  for $k = 1$ to innerIter **do**
    $P^{k+1} = \text{SoftTh}(\nabla(A^k)^T + B_1^k, \frac{\lambda_1}{\mu_1})$
    $Q^{k+1} = \text{Shrink}(A^k + B_2^k, \frac{\lambda_2}{\mu_2})$
    $S^{k+1} = \text{SoftTh}(MA^K - Y, \lambda_3)$
    $A^{k+1} = \text{mat}(a)$ from (10)
    $B_1^{k+1} = B_1^k + D_h X^{k+1} D - P^{k+1}$
    $B_2^{k+1} = B_2^k + D_v X^{k+1} D - Q^{k+1}$
  end for
  $Y = Y - MA^k - S^k$
end for
return $\hat{A} = A^{j+1}$

4. Results and Discussions

This section describes the details of various experiments executed to validate the proposed method. Firstly, datasets used in the experiments are described followed by evaluation metrics. After that, various synthetic data experiments and real data experiments are detailed with analysis of results.

A. Data Description

The existing USGS spectral library [35] was utilized in all the experiments. The library contains spectral signatures under six categories namely artificial, coatings, minerals, liquids, soil, and vegetation. We utilized endmembers from each of these categories in the experiments. We manually checked each endmember signature and removed some of the endmembers that had missing values for some wavelengths. Experiments were conducted with two synthetic and one real dataset. The first synthetic dataset has five abundance maps of 50×50 pixels with constant fraction value over a region. Each abundance map is composed of two or three endmembers as represented by the number of rectangular boxes inside a map. Dark blue background color represents zero-pixel value. Five endmembers were randomly selected to generate first synthetic image of dimension 50×50×224. The second synthetic dataset was generated using HYDRA toolbox [36]. Four abundance maps of size 128×128 were generated using Legendre method. The second synthetic image of dimension 128×128×224 was generated using four randomly selected endmembers from the spectral library. Both the datasets satisfy abundance sum to one constraint as well as abundance nonnegativity constraint. The experiments on the first synthetic image were conducted with the endmember matrix of dimension $R^{224\times269}$ such that angle between any two spectral signatures was at least 4◦. The experiments with second synthetic image do not make any such assumption and utilized endmember matrix of dimensions $R^{224\times889}$.

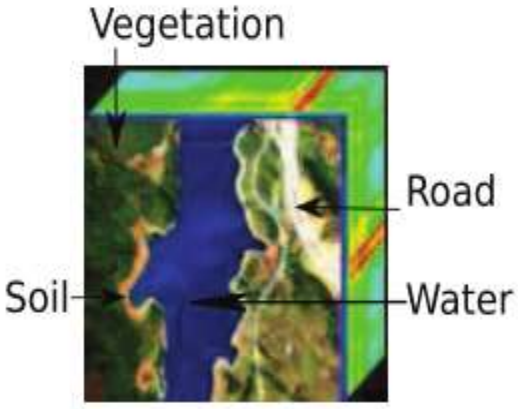

Figure 1. Data description with end member's diagram.

Real data experiments were done with a portion of Jasper Ridge image [37] of size $112 \times 118 \times 224$. A false color composite image is shown in Fig. 1. Several bands in this image are noisy bands. We had considered all 224 bands in real data experiments as opposed to many unmixing algorithms that remove noisy bands before doing unmixing. We did not have actual abundance maps for this real dataset; however, four major constituent endmembers can be easily recognized by visual interpretation. These four endmembers are roads, vegetation, soil, and water as indicated in Fig. 1.

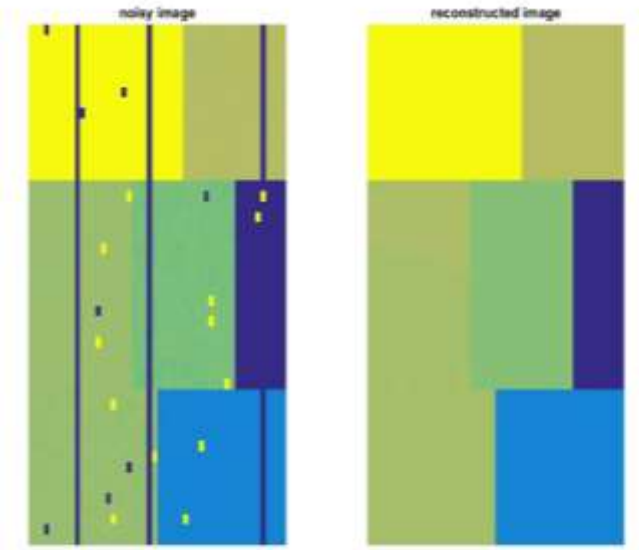

Figure 2. Noisy image and reconstructed image.

- PSNR of noisy image= 8.997199
- Elapsed time is 21.914467 seconds.
- Reconstructed Abundance PSNR=41.502979
- Reconstructed Image PSNR= 43.661829

5. Conclusion

We suggested a new method for hyperspectral unmixing in this work. In the generalised noise model, which contributes for specifically sparse noise, the joint sparsity and partial smoothness of the cartoons are manipulated in this approach. The supremacy of the new method over existing methods is suggested by experimental studies. The combined use of both complete regularization of variants and Split regularisation is not redundant since these fulfil different goals. Smooth mapping has been explored by regularisation of total variation. Although joint sparsity exploits the fact that where present, an end member is present in the same region in different positions. The latest USGS spectral library for spectrary signatures has been used for this work. In the current library, the spectral signatures may be different from the spectral signatures in the image. True images may also have non-spectral signature members of current libraries, so we expand the work to guide the hyperspectral image end signatures.

References

[1]. Ye, Chuanlong, et al. "Combining low-rank constraint for similar superpixels and total variation sparse unmixing for hyperspectral image." International Journal of Remote Sensing 43.12 (2022): 4331-4351.

[2]. Parente, Mario, and Marian-Daniel Iordache. "Sparse unmixing of hyperspectral data: The legacy of SUnSAL." 2021 IEEE International Geoscience and Remote Sensing Symposium IGARSS. IEEE, 2021.

[3]. 3.L. Ren, D. Hong, L. Gao, X. Sun, M. Huang and J. Chanussot, "Orthogonal Subspace Unmixing to Address Spectral Variability for Hyperspectral Image," in IEEE Transactions on

Geoscience and Remote Sensing, vol. 61, pp. 1-13, 2023, Art no. 5501713, doi: 10.1109/TGRS.2023.3236471.

[4]. Zhang, Shaoquan, et al. "Recent advances in hyperspectral unmixing using sparse techniques and deep learning." Hyperspectral Image Analysis: Advances in Machine Learning and Signal Processing (2020): 377-405.

[5]. Xu, Xia, and Zhenwei Shi. "Multi-objective based spectral unmixing for hyperspectral images." ISPRS Journal of Photogrammetry and Remote Sensing 124 (2017): 54-69.

[6]. Bioucas-Dias, José M., and Antonio Plaza. "An overview on hyperspectral unmixing: Geometrical, statistical, and sparse regression based approaches." 2011 IEEE International Geoscience and Remote Sensing Symposium. IEEE, 2011.

[7]. Iordache, Marian-Daniel, Antonio Plaza, and José Bioucas-Dias. "Recent developments in sparse hyperspectral unmixing." 2010 IEEE International Geoscience and Remote Sensing Symposium. IEEE, 2010.

[8]. Sara, Dioline, et al. "Hyperspectral and multispectral image fusion techniques for high resolution applications: A review." Earth Science Informatics 14.4 (2021): 1685-1705.

[9]. Shi, Chen, and Le Wang. "Incorporating spatial information in spectral unmixing: A review." Remote Sensing of Environment 149 (2014): 70-87.

[10]. Feng, Xin-Ru, et al. "Hyperspectral unmixing based on nonnegative matrix factorization: A comprehensive review." IEEE Journal of Selected Topics in Applied Earth Observations and Remote Sensing (2022).

[11]. Iordache, Marian-Daniel, Antonio Plaza, and José Bioucas-Dias. "Recent developments in sparse hyperspectral unmixing." 2010 IEEE International Geoscience and Remote Sensing Symposium. IEEE, 2010.

[12]. Quintano, Carmen, et al. "Spectral unmixing." International Journal of Remote Sensing 33.17 (2012): 5307-5340.

[13]. Jamshid Moghadam, H., and M. Mohammady Oskuei. "An Overview of Nonlinear Spectral Unmixing Methods in the Processing of Hyperspectral Data." Journal of Geomatics Science and Technology 10.1 (2020): 1-26.

[14]. Wang, Le, et al. "A survey of methods incorporating spatial information in image classification and spectral unmixing." International Journal of Remote Sensing 37.16 (2016): 3870-3910.

[15]. Hong, Danfeng, et al. "An augmented linear mixing model to address spectral variability for hyperspectral unmixing." IEEE Transactions on Image Processing 28.4 (2018): 1923-1938.

[16]. Wan, Lulu, et al. "Hyperspectral unmixing based on spectral and sparse deep convolutional neural networks." IEEE Journal of Selected Topics in Applied Earth Observations and Remote Sensing 14 (2021): 11669-11682.

[17]. Halimi, Abderrahim, Paul Honeine, and Jose M. Bioucas-Dias. "Hyperspectral unmixing in presence of endmember variability, nonlinearity, or mismodeling effects." IEEE Transactions on Image Processing 25.10 (2016): 4565-4579.

[18]. He, Wei, Hongyan Zhang, and Liangpei Zhang. "Total variation regularized reweighted sparse nonnegative matrix factorization for hyperspectral unmixing." IEEE Transactions on Geoscience and Remote Sensing 55.7 (2017): 3909-3921.

[19]. Zhao, Min, et al. "A plug-and-play priors framework for hyperspectral unmixing." IEEE Transactions on Geoscience and Remote Sensing 60 (2021): 1-13.

[20]. Zhou, Lei, et al. "Subspace structure regularized nonnegative matrix factorization for hyperspectral unmixing." IEEE Journal of Selected Topics in Applied Earth Observations and Remote Sensing 13 (2020): 4257-4270.